JACS Au
AN OPEN ACCESS JOURNAL OF THE AMERICAN CHEMICAL SOCIETY

pubs.acs.org/jacsau
Article

Deciphering the Diffusion-Improved Selectivity of Ethylene Mediated by the Mesoscale Spatial Pattern of Aromatics in Zeolite-Catalyzed Methanol-to-Olefin Processes

Qingteng Chen, Jian Liu, and Bo Yang*

Cite This: JACS Au 2025, 5, 1791−1802
Read Online

ACCESS | Metrics & More | Article Recommendations | Supporting Information

ABSTRACT: Modeling the diffusion behavior of nonuniformly distributed systems at the mesoscopic scale presents significant challenges. In this study, we investigate how the nonuniform mesoscale spatial distribution of aromatic compounds, i.e., the hydrocarbon pool, affects olefin selectivity during the methanol-to-olefins (MTO) process. Ab initio molecular dynamics with enhanced sampling methods and kinetic Monte Carlo techniques were employed to analyze olefin diffusion in a "fully filled from the outside to the inside" distribution model. Our results reveal that while the coexistence of olefins with aromatic compounds hinders olefin diffusion, it simultaneously enhances ethylene selectivity. Further analysis of diffusion rate control and olefin residence time distributions within the zeolite model identifies key elementary diffusion processes and elucidates why aromatic compounds preferentially form at the rim of the SAPO-34 zeolite during the MTO process. This integrated approach enables the simulation of catalytic systems over larger spatial and temporal scales, providing a comprehensive understanding of the underlying mechanisms and facilitating the design of more efficient and ethylene-selective catalysts.

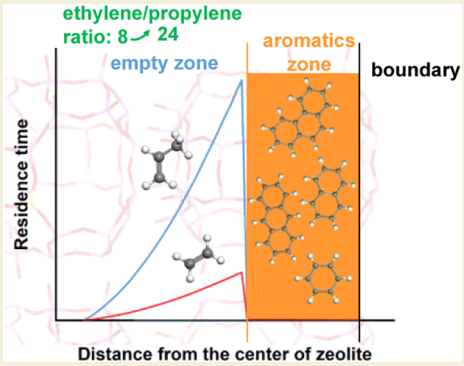

KEYWORDS: *ab initio molecular dynamics, diffusion, zeolite, olefin, kMC*

1. INTRODUCTION

Light olefins ($C_2^=$ ∼ $C_4^=$) play a crucial role as industrial raw materials, serving as the building blocks for the production of various chemicals, including synthetic textiles and packaging materials.[1] Traditionally, light olefins have been predominantly derived from steam cracking and fluid catalytic cracking of naphtha in the petroleum industry.[2−4] However, given the depletion of fossil fuels, there is a pressing need to explore nonpetroleum pathways for the synthesis of light olefins. One such alternative route is the methanol-to-olefins (MTO) process, which utilizes methanol produced from either natural gas, coal, or biomass as a reactant to produce ethene and propene.

The widely accepted reaction mechanism for the MTO process is the hydrocarbon pool (HCP) mechanism, where trapped organic molecules serve as cocatalysts in the formation of olefins.[5−11] This mechanism comprises two reaction cycles: the olefin-based cycle, in which olefins undergo methylation and cracking reactions to generate more olefins; and the cycle involving aromatic compounds as HCP species, which encompasses two different reaction mechanisms, namely, the side-chain mechanism and the paring mechanism. In the side-chain mechanism, an alkyl chain is formed through methylation reactions, followed by the elimination of the alkyl chain to form olefin molecules. In contrast, the pairing mechanism involves the growth of the alkyl chain through ring contraction/expansion reactions.

The MTO process occurs in acidic zeolite and zeotype catalysts, with SAPO-34 zeolite demonstrating high selectivity toward light olefins due to its unique structure.[12] SAPO-34 features the CHA topology, characterized by spacious cages connected by small eight-membered-ring (8MR) windows. The presence of large aromatic compounds within its spacious cages, coupled with the limiting diffusion of large species through the 8MR window, contributes to the achievement of a high selectivity for light olefins. In SAPO-34 zeolite, the aromatics-based cycle is preferred, and the active HCP species is methylbenzenes (MBs), with calculations performed by Wang et al. indicating that tetramethylbenzene (TMB) is the most active species.[5] Experimental results suggested that these aromatic compounds tend to form at the rim of the SAPO-34 zeolite, inhibiting both the diffusion of the reactant (methanol) into the zeolite and the diffusion of the products (olefins) out

Received: January 14, 2025
Revised: February 28, 2025
Accepted: March 3, 2025
Published: April 1, 2025

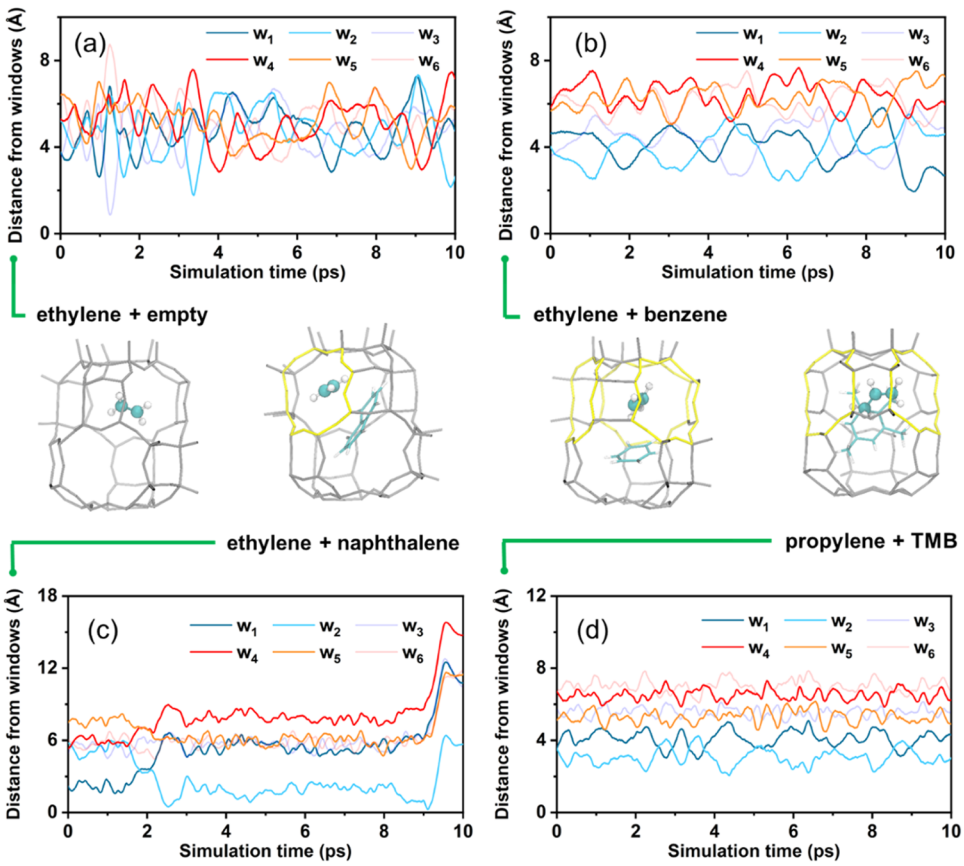

Figure 1. Identification of the stable sites of olefins coexisting with different aromatic compounds in the SAPO-34 cage. The distance between the olefins and the six 8MR windows ($w_1 \sim w_6$) in the SAPO-34 cage varies with the MD simulation time when olefins coexist with different aromatic compounds: (a) ethylene, (b) ethylene and benzene, (c) ethylene and naphthalene, and (d) propylene and TMB. The yellow sticks in the inserted zeolite models represent the closest 8MR windows to the olefin.

of the zeolite. Obviously, the product selectivity will be influenced due to the different diffusion resistance to different products.[13−15]

As the reaction time increases, MBs are further converted to polycyclic aromatic hydrocarbons (PAHs), such as naphthalene, phenanthrene, and anthracene, and the ethylene/propylene ratio also increases simultaneously.[7,8,16] These PAHs are considered precursors of carbon deposits.[17,18] Recent results reported by Zhou et al. have indicated that polymethylnaphthalene can also act as an HCP species and participate in the MTO process, achieving high ethylene selectivity through the coupling of reaction and diffusion.[13]

In HSAPO-34 zeolite, a typical three-dimensional (3D) porous material, the simultaneous occurrence of reaction and diffusion poses significant challenges in isolating their individual effects through experimental methods. While theoretical simulations can provide insights into the free energy profile and reaction rate of elementary reactions, determining the influence of the nonuniform distribution of aromatic compounds within zeolite on reactivity and product selectivity at the mesoscopic scale remains problematic.

The conventional approach to investigating diffusion behavior over large spatial scales involves constructing a cell containing a finite number of molecules, conducting force field molecular dynamics (FF-MD) with periodic boundary conditions, and calculating the self-diffusion coefficient of the molecule from the mean square displacement.[19,20] However, the simulation results of FF-MD are not sufficiently accurate. Cnudde et al. have pointed out that FF-MD is unable to depict the promotional effect of acid sites in the 8MR window on the diffusion of olefins.[21] Furthermore, the impact of the mesoscale spatial pattern of aromatic compounds within the zeolite on olefin diffusion cannot be adequately considered due to the limited cell size. Therefore, a new approach to simulate the evolution of nonuniform distributed system over larger spatial and temporal scales is urgently needed.

In the previous literature, the impact of the reaction process on product selectivity has been extensively studied.[5,6,9] However, the effect of the mesoscale spatial pattern of aromatics on the diffusion process is still unclear. In the current work, ab initio molecular dynamics (AIMD) is utilized to identify the elementary diffusion processes when olefins coexist with different aromatic compounds within SAPO-34 zeolite, and the corresponding free energy profiles are obtained through enhanced free energy sampling methods. Then the free energy barriers are integrated with the kinetic Monte Carlo (kMC) method to assess the quantitative impact of different mesoscale spatial patterns of aromatic compounds on olefin diffusion and ethylene/propylene selectivity.

2. RESULTS AND DISCUSSION

2.1. Elementary Diffusion Processes and Free Energy Profiles

In order to investigate the states in which olefins coexist with different types of MBs and PAHs, including benzene,

https://doi.org/10.1021/jacsau.5c00045
JACS Au 2025, 5, 1791−1802

naphthalene, phenanthrene, anthracene, and TMB (the formers are typical monocyclic, bicyclic, and tricyclic aromatics, and TMB serves as a highly reactive intermediate in the MTO process), in the cage of SAPO-34, regular AIMD simulations were performed. The 1 × 1 × 1 and 1 × 2 × 1 SAPO-34 models were employed to simulate diffusion processes within the cage and between adjacent cages, respectively (see Figure S1). The effect of Brønsted acid sites (BAS) is not considered in this work due to the complex interactions between BAS and both olefins and benzene rings.[21,22]

Initially, a series of 10 ps regular AIMD simulations were conducted to gather key structural information in the 1 × 1 × 1 SAPO-34 model. Subsequent enhanced sampling simulations confirm that 10 ps AIMD simulations are sufficient to sample the stable sites of olefins in SAPO-34. Figure 1 depicts the distances between the centroid of olefin and the six 8MR windows as a function of simulation time. Figure 1a illustrates that when ethylene is present in an empty cage, it can move freely within this cage and has an equal probability of contacting all six 8MR windows. Due to the high free energy barrier for intercage diffusion, the unhindered movement of ethylene in the cage can be considered a rapid process. Therefore, ethylene has only one stable site in the empty cage and can diffuse through one of the six 8MR windows to another stable site in the adjacent cage. This site-to-site hopping process can be regarded as an elementary diffusion process.

In accordance with the work of Cnudde et al.,[23] the height of the olefin centroid from the plane in which the 8MR window is located was utilized as the collective variable (CV) (Figure 2a,b), and the free energy profiles of the intercage diffusion of olefins between two adjacent empty cages, defined as the "empty−empty" process (Figure 2e), were obtained and are presented in Section S2 of Supporting Information. The diffusion free energy barriers of ethylene and propylene for the "empty−empty" process are 31.1 and 42.7 kJ/mol, respectively, consistent with the fact that propylene is larger in size than ethylene.

When ethylene and benzene coexist in a cage, as depicted in Figure 1b and the corresponding structure, it is observed that ethylene and benzene are situated on opposite sides of the cage. This arrangement is due to the comparable size of benzene (7.0 Å based on the Fisher−Hirschfelder−Taylor hard sphere molecular model) to the size of the cage (10 × 6.7 Å).[24,25] Ethylene has an equal probability of contacting the three 8MR windows on the same side, indicating that it has two equivalent stable sites in the cage. Ethylene or propylene can reach the stable site of adjacent cages through intercage diffusion via the closest three 8MR windows; the diffusion free energy barriers of "benzene-empty" process are 20.4 and 29.1 kJ/mol, respectively. The diffusion free energy barriers of its inverse process ("empty-benzene" process) are 33.1 and 50.7 kJ/mol, respectively. These barriers are higher than those of the "empty−empty" process (31.1 and 42.7 kJ/mol), which may be attributed to the interaction between the olefins and benzene.

It should be noted that ethylene or propylene can also swap positions with benzene through an intracage diffusion process (see Figure S6). However, due to the relatively high diffusion free energy barrier of this process, it is difficult to observe in a 10 ps MD simulation. Therefore, an enhanced sampling method is applied, and the centroid of the olefin along the *z*-axis is set as the CV (Figure 2c). The diffusion free energy barriers of ethylene and propylene are 20.7 and 28.6 kJ/mol, respectively, for the intracage-benzene process, which are similar to the barriers of the "benzene-empty" process (20.4 and 29.1 kJ/mol). This similarity indicates that when ethylene or propylene coexists with benzene in the cage, the probabilities of intercage diffusion and intracage diffusion are similar.

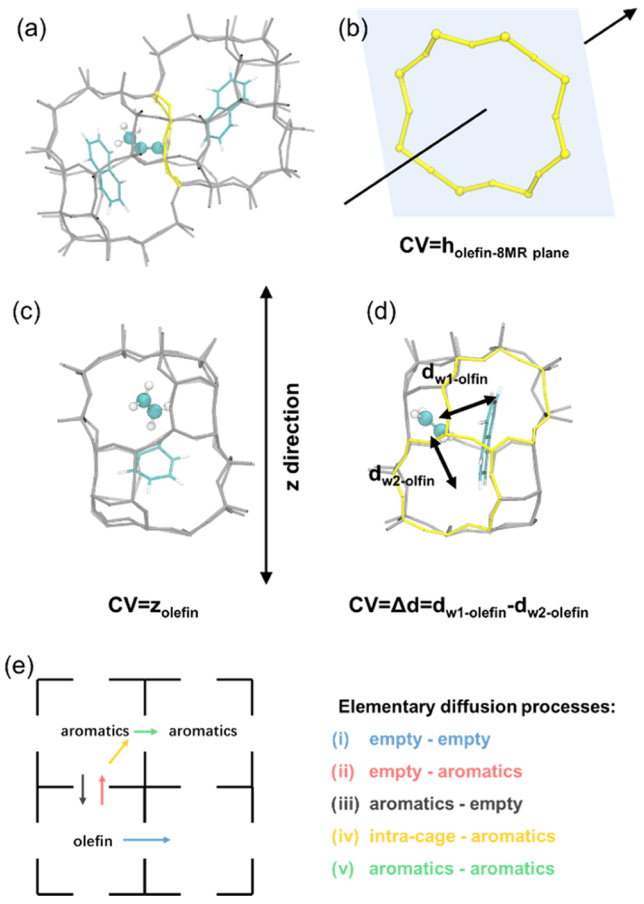

Figure 2. Elementary diffusion processes and corresponding collective variables. (a−d) Schematic diagram of the collective variables applied in blue-moon sampling of the free energies based on AIMD simulations. The gray sticks represent the zeolite framework, while the yellow 8MR window and olefin in the ball-and-stick model represent atoms associated with the collective variables. (e) Schematic diagram of the five elementary diffusion processes.

As the size of aromatic compounds increases, the space for the free movement of olefins is further compressed when olefins coexist with naphthalene, phenanthrene, or anthracene in a cage. In Figure 1c, it is observed that ethylene is localized around one of the six 8MR windows, with the same distance from the four adjacent windows and the farthest distance from the opposite window. This indicates that there are six equivalent stable sites for olefins in the cage. It can reach the adjacent stable sites by an intracage diffusion process, and due to the low diffusion free energy barrier, this process occurs at 2 ps, as shown in Figure 1c. Olefins can also diffuse to the adjacent cage through the closest 8MR window, and this process occurs at 9 ps in Figure 1c. The diffusion free energy barriers of the "empty−aromatics" process for ethylene with the aromatic compounds being naphthalene, phenanthrene, and anthracene are 35.5, 37.4, and 33.2 kJ/mol, respectively.

https://doi.org/10.1021/jacsau.5c00045
JACS Au 2025, 5, 1791−1802

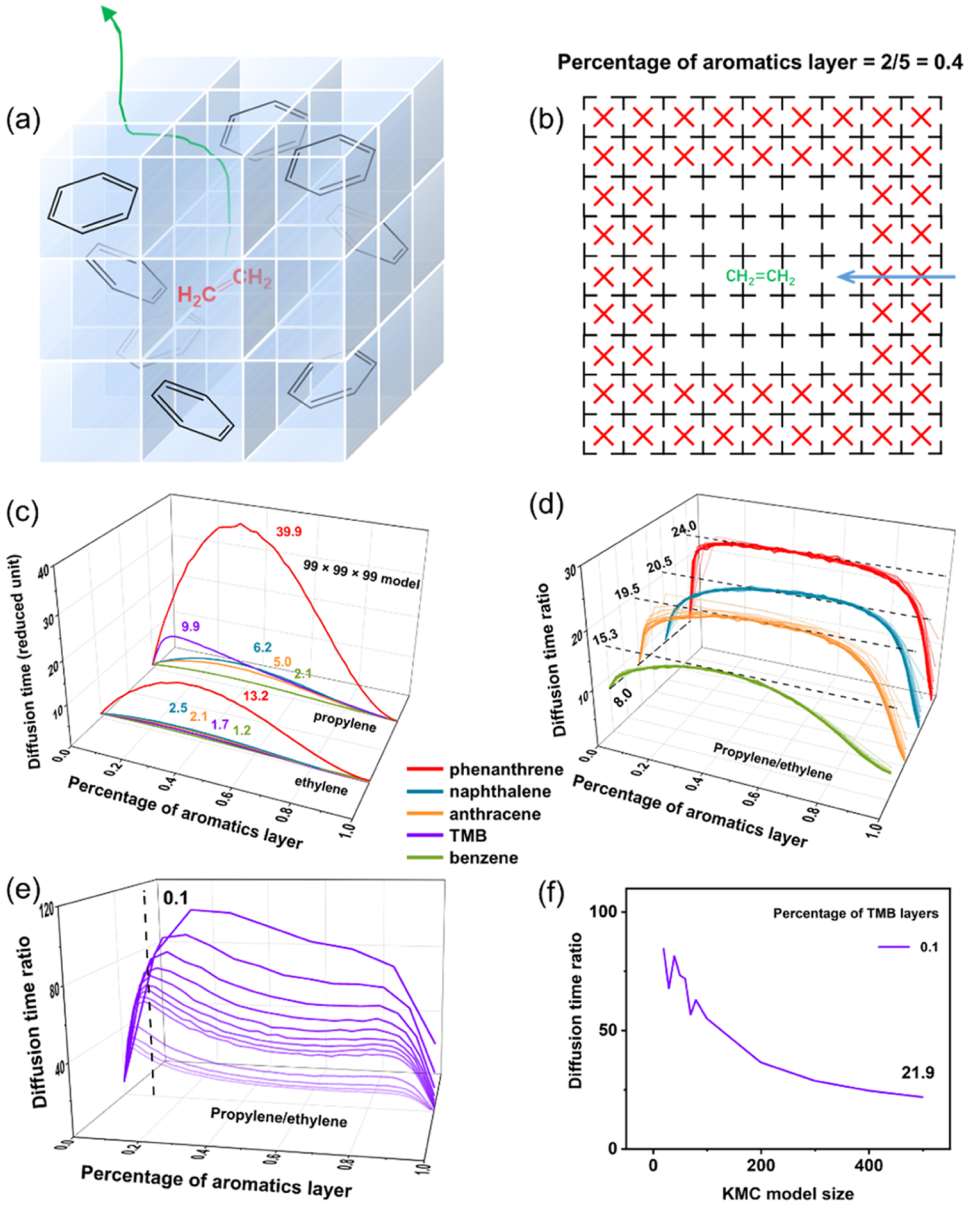

Figure 3. Model applied in kinetic Monte Carlo simulations, and the diffusion behaviors of olefins coexist with different aromatic compounds. (a, b) Schematic diagram of the 3D "cubic" model and the distribution described as "fully filled from the outside to the inside". (c) Diffusion time (reduced unit) of ethylene or propylene coexists with different aromatic compounds as a function of the percentage of aromatics layer in 99 × 99 × 99 "cubic" model. (d, e) The diffusion time ratio of propylene to ethylene coexists with different aromatic compounds varies with the percentage of aromatics layer in different sizes of "cubic" model. (f) Diffusion time ratio of propylene to ethylene varies with "cubic" model size when the percentage of TMB layer = 0.1.

The corresponding free energy barriers of the "intra-cage-aromatics" process are 9.4, 19.9, and 13.2 kJ/mol, respectively. The free energy barriers of elementary diffusion processes involving phenanthrene are the highest. The same result is also present when propylene is applied as the diffusion molecule, which may be due to the larger kinetic diameter of phenanthrene.

When ethylene and TMB coexist in a cage, ethylene is also localized around one 8MR window. However, when propylene coexists with TMB, its stable site changes. Figure 1d shows that the stable site is located in the middle of the two adjacent 8MR windows and propylene has the same probability of touching the two closest 8MR windows. This means that it can diffuse through these two windows to the adjacent cage or diffuse to another equivalent stable site through intracage diffusion. The diffusion free energy barriers of "TMB-empty" and "intra-cage-TMB" processes are relatively low (9.6 and 5.2 kJ/mol, respectively).

Based on the above results, when only one olefin molecule and several aromatic compounds are present in SAPO-34, and assuming that aromatic compounds cannot diffuse through the narrow 8MR window and that one cage can only accommodate one aromatic molecule, the entire diffusion process of olefin can be divided into a finite number of elementary diffusion processes. These elementary diffusion processes can be categorized into five distinct types, as shown in Figure 2e, namely "empty−empty," "empty−aromatics," "aromatics−empty," "aromatics−aromatics," and "intra-cage-aromatics" processes. When only one type of aromatic compound is contained in SAPO-34, the number of elementary diffusion

https://doi.org/10.1021/jacsau.5c00045
JACS Au 2025, 5, 1791−1802

processes is further reduced to 5, and all of the free energy barriers calculated are listed in Table S1. This approach can simplify the diffusion behavior of olefins and assist in considering the diffusion of olefins at mesoscale.

2.2. Kinetic Monte Carlo Simulations

If the diffusion process of olefins in SAPO-34 can be divided into finite hops from one stable site to an adjacent stable site, then the free energy barriers of these elementary diffusion processes can be used in combination with the kinetic Monte Carlo technology to further investigate the influence of the mesoscale spatial pattern of aromatic compounds on the diffusion of olefin.

As mentioned above, SAPO-34 features the CHA topology, in which spacious cages are connected by small 8MR windows and each cage contains six 8MR windows. Therefore, it is reasonable to apply the "cubic" model to represent SAPO-34 zeolite (see Figure 3a). To further simplify the model, only one kind of aromatic hydrocarbon is placed in the "cubic" model each time the kMC simulation is performed, resulting in only five elementary diffusion processes in the event list.

The mesoscale spatial pattern of aromatic compounds in the "cubic" model is based on the experimental results in the literature,[13,14] specifically the "fully filled from the outside to the inside" distribution (Figure 3b), with further details provided in the Methods section. The unfilled area inside is named "empty zone," and the filled area on the outside is named "aromatics zone", and these concepts will be used in the subsequent discussion. The percentage of aromatic layers in the total number of layers in the "cubic" model is varied to observe changes in olefin diffusion time. According to the literature, the maximum proportion of HSAPO-34 cages occupied by MBs reaches 25% during the MTO process, with polycyclic aromatics present at 3−6 times higher (in wt %) than that amount of MBs.[7] Therefore, when the percentage of aromatics layers is 0.1−0.2, zeolite can be considered with high activity.

The effect of different mesoscale spatial patterns of various aromatic compounds on the diffusion time of olefins is considered first, and the corresponding results are shown in Figure 3c. The 99 × 99 × 99 "cubic" model is employed here, and the diffusion time of the corresponding olefin in the empty "cubic" model is used as the reference to obtain the reduced unit diffusion time. Figure 3c illustrates that as the percentage of aromatics layers increases, the diffusion time (reduced unit) exhibits a peak-shaped curve.

The impeding effect of benzene on ethylene or propylene diffusion is weak, with peak values of the diffusion time (reduced units) at only 1.2 and 2.1, respectively. This is attributed not only to the similarity of the free energy barriers of the "empty−empty" (31.1 and 42.7 kJ/mol) and "empty−benzene" processes (33.1 and 50.7 kJ/mol) but also to the presence of more intercage diffusion paths for olefins, allowing them to diffuse through the benzene region even without undergoing the "intra-cage-benzene" process.

When the aromatic compounds in the "cubic" model are naphthalene, phenanthrene, anthracene, or TMB, the olefins must undergo continuous "empty−aromatics" and "intra-cage-aromatics" processes to cross the interface of the empty zone and aromatics zone, resulting in a higher effective free energy barrier than the "empty−empty" process and a longer diffusion time. However, for ethylene, except for phenanthrene, the diffusion resistance from other aromatic compounds is limited and the highest peak value is only 2.5. For propylene, the diffusion resistance is stronger, indicating that the introduction of aromatic compounds will improve the selectivity of ethylene.

The effect of different mesoscale spatial patterns of various aromatic compounds on olefin selectivity is further explored. The size of the "cubic" model ranges from 9 × 9 × 9 to 99 × 99 × 99, and the olefin selectivity is demonstrated by the ratio of the diffusion time of propylene to ethylene. The higher this ratio is, the higher the selectivity of ethylene will be. Figure 3d illustrates that in the empty model the diffusion time ratio is about 8.0, indicating that the introduction of aromatic compounds does improve the selectivity of ethylene. For benzene, naphthalene, phenanthrene, and anthracene, with different sizes of the "cubic" model, the diffusion time ratio curves with the percentage of aromatics layers are almost overlapped. This indicates that the selectivity may be independent of the size of SAPO-34 zeolite but only dependent on the percentage of aromatics layers when olefins coexist with the above aromatic compounds.

When the aromatic compound is benzene, the curve of the diffusion time ratio is also peak-shaped, with the peak value at 15.3 occurring at a percentage of benzene layers of about 0.4. When the aromatic compound is naphthalene, phenanthrene, or anthracene, the curve is plateau-shaped, and the diffusion time ratio fluctuates only slightly over a wide range, between 0.2 and 0.7 of the percentage of aromatics layers. This means that as long as these percentages of aromatics layers reach the threshold, the highest ethylene selectivity can be maintained over this wide range. When the aromatic compound is TMB, the situation is slightly different. The diffusion time ratio decreases as the size of the "cubic" model increases, and the results are shown in Figure 3e.

A series of supplementary kMC simulations are performed, and the size of the "cubic" model is further increased to 199 × 199 × 199−499 × 499 × 499. Considering that the zeolite has high activity when the percentage of aromatics layers is 0.1, the diffusion time ratio of propylene to ethylene with the size of the "cubic" model is collected at this percentage of aromatics layers (0.1) and shown in Figure 3f. When the zeolite model size is increased to 499, the diffusion time ratio decreases from ∼80 to 21.9, although it is still higher than the diffusion time ratio of the empty model (∼8.0). Considering that TMB is a highly active HCP species as reported in the literature,[5] the degree of diffusion resistance of TMB to olefins will greatly affect the product selectivity during the steady-state period of the MTO process.[26] The simulation results show that the use of a smaller size SAPO-34 zeolite will further improve the selectivity of ethylene, coupled with a slower deactivation rate that smaller size SAPO-34 zeolites show. Additionally, it should be noted that the distance between the centroids of two adjacent cages is approximately 9.3 Å; therefore, the 499 × 499 × 499 model corresponds to a SAPO-34 crystal with an approximate size of 0.46 μm.

One can find from the above results that the introduction of aromatic compounds will hinder the diffusion of olefins but will also improve the selectivity of ethylene. For example, phenanthrene has the strongest ability to hinder diffusion but can also achieve the highest ethylene selectivity (24.0). The introduction of naphthalene is a better choice to achieve high ethylene selectivity (20.5), while it only slightly interferes with olefin diffusion, which is consistent with experimental results.[13]

https://doi.org/10.1021/jacsau.5c00045
JACS Au 2025, 5, 1791−1802

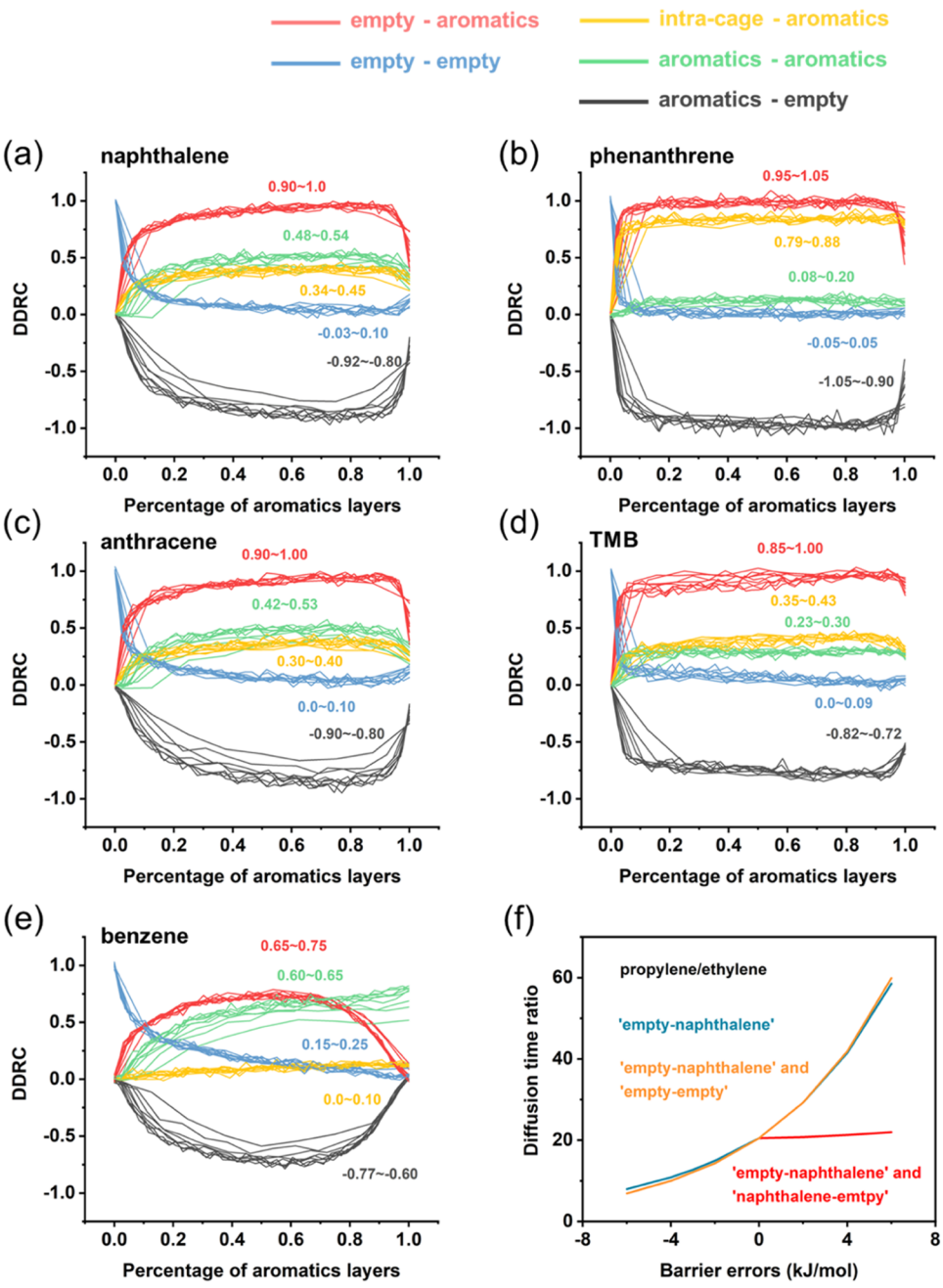

Figure 4. DDRC analysis of different elementary diffusion processes. (a−e) DDRC values of five elementary diffusion processes vary with the percentage of aromatics layers. (f) Within the uncertainty range, the diffusion time ratio of propylene to ethylene varies with the free energy barriers of different elementary diffusion processes.

2.3. Degree of Diffusion Rate Control (DDRC) Analysis

In order to explore the influence of these elementary diffusion processes on diffusion time, we introduce a new indicator. The degree of rate control (DRC) is a parameter often used to evaluate the influence of changes in the barrier of a given elementary reaction on the total reaction rate in a complex reaction network. Here, this concept is borrowed to evaluate the effect of the perturbation of the free energy barrier of the elementary diffusion process on the diffusion time, which is named the degree of diffusion rate control (DDRC, for the elementary diffusion process i, $\mathrm{DDRC}_i = (\partial \ln(1/t)/\partial(-G_{a,i}/RT))_{G_{a,j\neq i}}$), with further details provided in the Methods section. Because the DDRC values of olefins are similar (Figure S7), only the case of propylene is considered here, and the corresponding results are shown in Figure 4.

As illustrated in Figure 4a−d, when the aromatic compounds are naphthalene, phenanthrene, anthracene, or TMB, the DDRC results exhibit similar trends, and their values are found to be independent of the percentage of aromatic layers over a wide range (0.2−0.9). The "empty−aromatics" and "aromatics−empty" processes have the most significant impact on the diffusion time. This is because these two processes are effectively the inverse of each other; an increase in the free energy barrier of the former will lead to an increase in the diffusion time, while the latter has the opposite effect. The DDRC value of the "empty−empty" process is 0. From a macroscopic perspective, the diffusion of olefins away from the

https://doi.org/10.1021/jacsau.5c00045
JACS Au 2025, 5, 1791−1802

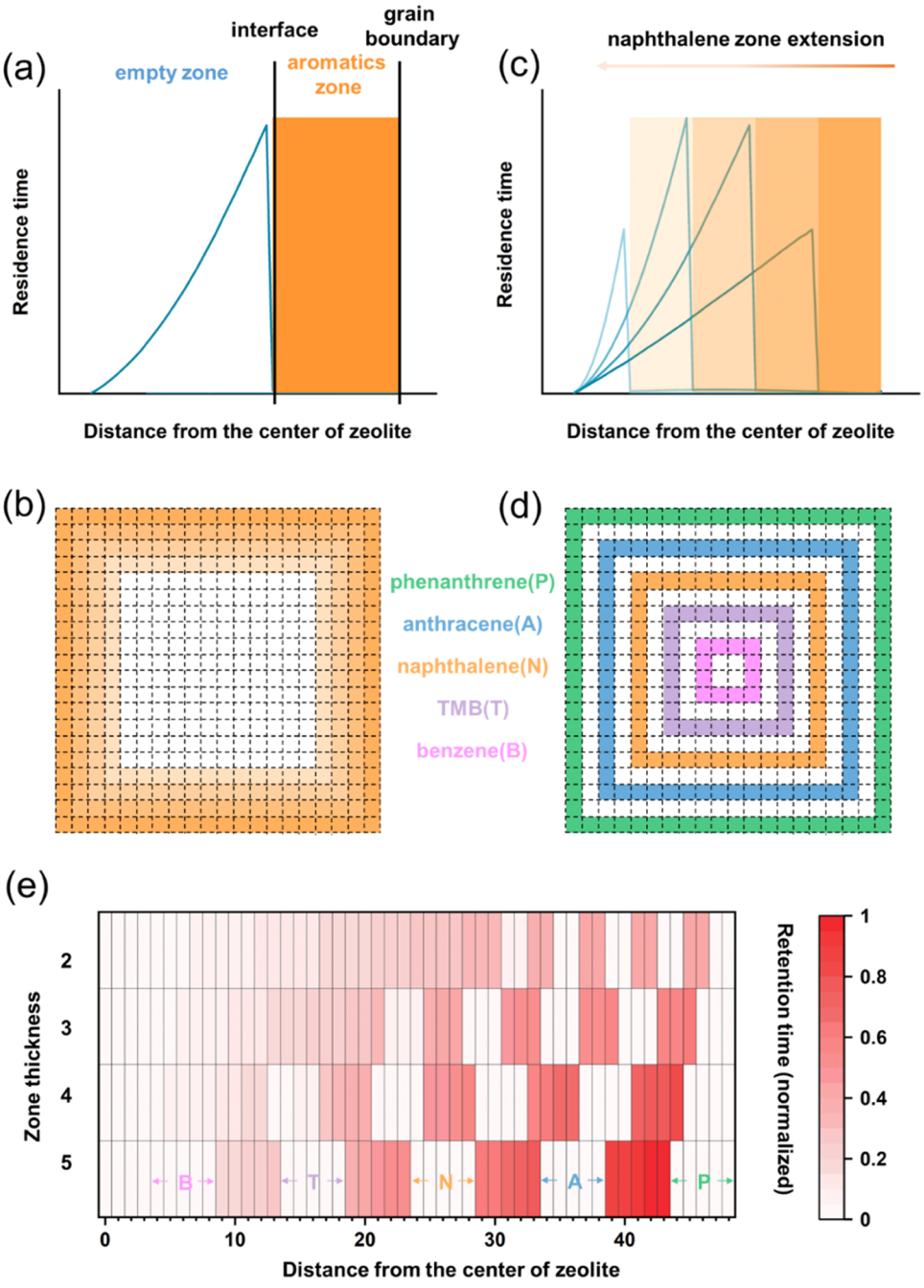

Figure 5. Ethylene residence time distribution under different mesoscale spatial patterns of aromatic compounds. (a) Schematic diagram of the residence time distribution of olefins in the "cubic" model. (b) Schematic diagram of naphthalene zone extension and (c) the corresponding ethylene residence time distribution variation. (d) Schematic diagram of alternating aromatics zones and empty zones model and (e) the corresponding ethylene residence time distribution variation.

"cubic" model necessitates sequential passage through the empty and aromatic zones, and the process of crossing the interface between these two zones resembles a rate-controlling step. The residence time of the olefin in the empty zone depends solely on the rate of the crossing process; consequently, the perturbation of the free energy barrier of the "empty−empty" process has no impact on the diffusion time. The DDRC values of the intracage−aromatics and "aromatics−aromatics" processes are positive, as both processes macroscopically impede the passage of olefins across the aromatic zone.

When the aromatic compound is benzene, the situation exhibits some distinctions. As depicted in Figure 4e, there is a correlation between the DDRC values and the percentage of aromatic layers. The "empty−benzene" and "benzene−empty" processes continue to have the most significant impact on the diffusion time. However, the DDRC values of the "intra-cage-benzene" process drop to 0. This is because olefins do not need to undergo the "intra-cage-benzene" process to diffuse away from the zeolite structure. Instead, the DDRC values of the "benzene−benzene" and "empty−empty" processes are positive, and with the increasing aromatic zone, the former increases, while the latter decreases.

https://doi.org/10.1021/jacsau.5c00045
JACS Au 2025, 5, 1791−1802

Error analysis of a series of free energy profiles indicates that the error in the free energy barriers of these elementary diffusion processes is primarily within the range of ±4 to ±6 kJ/mol (Table S1). Therefore, in the case of aromatic compounds, such as naphthalene, the "empty−naphthalene" process, which has the greatest impact on the diffusion time, is selected, and the influence of its free energy barrier within the uncertainty range on the selectivity of olefins is further explored. As shown by the blue curve in Figure 4f, the response of the diffusion time ratio of propylene to ethylene is nonlinear as the free energy barrier of this process changes. The lowest diffusion time ratio is 7.9, which is similar to the diffusion time in the empty model (8.0), while the highest is 58.5. This indicates that increasing the free energy barrier of the propylene "empty−naphthalene" process can effectively improve the selectivity of ethylene.

It is important to note that the free energy barriers of the five elementary diffusion processes are often interdependent. For instance, if the free energy barrier of the "empty-naphthalene" process is adjusted by changing the free energy of the initial state (olefin in empty cage), then the free energy barrier of the "empty−empty" process will also be adjusted simultaneously due to the changes in the free energy of the olefin in the empty cage. Nonetheless, since the perturbation of the free energy barrier in the "empty−empty" process has a negligible effect on the diffusion time, the results of the orange and blue curves in Figure 4f almost overlap.

Alternatively, if the free energy barrier of the "empty-naphthalene" process is adjusted by changing the free energy of the transition state, then the free energy barrier of its reverse process ("naphthalene-empty" process) will be adjusted simultaneously. Since the free energy barrier of the "naphthalene−empty" process is only 1.3 kJ/mol, only the increase of free energy of the transition state is considered here. As these two processes have opposite DDRC values, the change in the free energy of the transition state has a negligible effect on the selectivity of the olefins, as shown by the red curve in Figure 4f.

Given the possible interdependence of these elementary diffusion processes, it poses a significant challenge to selectively regulate the free energy barrier of a single process when modifying the zeolite structure by experimental means. Furthermore, the changes in the free energy barrier of certain processes may not necessarily translate to meaningful impacts on the final results. Therefore, it is prudent to first identify the key processes through computational simulations and subsequently focus on selectively modifying these critical processes in experimental studies. This strategic approach is more likely to yield the desired outcomes in terms of achieving high formation rates and selectivities for the target product.

2.4. Discussion

The prolonged residence time of olefins increases the probability of their further conversion to aromatic compounds. However, due to the inherent complexity of the reaction network involved, the distribution of the residence time of olefins in the "cubic" model can be employed as a rough representation of the probability of olefin conversion to aromatic compounds.

Prior to the steady state of the MTO process, olefins can diffuse freely within the SAPO-34 framework, while aromatic compounds have not yet formed. According to the existing literature, the zeolite framework possesses a stabilizing effect on olefins, resulting in an adsorption energy that impedes the diffusion of olefins away from the zeolite and into the gas phase.[27,28] This may lead to the formation of initial aromatic compounds by these trapped olefins in the subsurface pores of SAPO-34. Furthermore, the literature has reported that in some cases, the density of BAS in the outer layer of the zeolite is higher than that on the inside, and[29−32] this may also result in preferential formation of initial aromatic compounds at the rim of the zeolite. Once the initial aromatic zone is formed, the interface between the aromatic zone and the empty zone further acts as a grain boundary, thereby hindering the diffusion of olefins away from the zeolite.

In order to verify this hypothesis, the "cubic" model containing ethylene and naphthalene is selected, and the schematic diagram of the distribution of the ethylene residence time in the model is shown in Figure 5a. This figure illustrates that ethylene is predominantly trapped in the empty zone, and once it crosses the interface, it quickly diffuses away from the zeolite. The crossing process can be considered analogous to the rate-determining step in the reaction; consequently, olefins are uniformly distributed within the empty zone. In the cubic model, as one approaches the surface, the volume of the shell layer per unit distance increases, thereby favoring the localization of olefins at the interface, as shown in Figure 5a. Subsequently, the residence time distribution of ethylene was tested in models with varying thicknesses of the naphthalene zone, as depicted schematically in Figure 5b. The residence time distribution results (Figure 5c) indicate that regardless of the thickness of the naphthalene zone, the closer ethylene gets to the interface, the longer it resides there. This suggests that the interface sites hinder the diffusion of olefins and lead to an increased residence time in the vicinity of the interface, which in turn enhances the probability of further conversion of olefins to aromatic compounds and extends the aromatics zone inward.

From the above observations, it can be reasonably inferred that even if there are some voids within the aromatics zone, this area can be considered as a small "fully filled from the outside to the inside" distribution region, where olefins will also be trapped and converted to aromatic compounds at the interface, eventually filling these voids. To further validate this hypothesis and align it with the experimental observations, a new model is adopted (Figure 5d), in which alternating aromatic zones and empty zones are represented, with the aromatic compounds arranged in the order of increasing size from the inside to the outside, i.e., benzene, TMB, naphthalene, anthracene, and phenanthrene.

As shown in Figure 5e, when empty zones are contained within the aromatic zones, olefins will be trapped in these empty zones. Furthermore, the closer the olefins are to the grain boundary, the longer their residence time, indicating that olefins are preferentially converted to aromatic compounds and fill the empty zones of the outer layer, thereby eliminating the voids in the aromatic zone.

These results not only illustrate the rationality of the "fully filled from the outside to the inside" distribution model but also explain the observed tendency of aromatic compounds to form at the rim of the zeolite during the MTO process. The mesoscale spatial pattern of aromatic compounds governing the residence time and conversion of olefins within the heterogeneous zeolite system plays a crucial role in determining the evolution of the aromatics zone and, as introduced above, the selectivity of ethylene.

https://doi.org/10.1021/jacsau.5c00045
JACS Au 2025, 5, 1791−1802

3. CONCLUSIONS

In summary, the results show that when olefins coexist with aromatic compounds such as benzene, naphthalene, phenanthrene, or anthracene, the mesoscale spatial pattern of aromatic compounds, while hindering the diffusion of olefins, can also help improve the selectivity of ethylene. Importantly, the selectivity depends only on the percentage of aromatic layers but not on the size of the SAPO-34 zeolite when olefins coexist with the above aromatic compounds. However, when olefins coexist with TMB, the selectivity of ethylene decreases with an increase in the size of the SAPO-34 zeolite. This suggests that the use of smaller SAPO-34 zeolites not only helps to slow the deactivation rate but also contributes to enhancing the selectivity of ethylene. A new indicator, DDRC is proposed, and the analysis indicates that the perturbation of the free energy barriers of the "aromatics−empty" and "empty−aromatics" diffusion processes has the greatest impact on the diffusion time. Therefore, manipulating the free energy barriers of these key elementary diffusion processes, such as by adjusting the pore size, can be a viable strategy to improve the formation rate and selectivity of the target product. And the residence time distribution of olefins in the model is analyzed to explain the experimental observation that aromatic compounds are preferentially formed at the rim of SAPO-34 zeolite, as well as to validate the rationality of the "fully filled from the outside to the inside" distribution model. The combination of AIMD and kMC technologies can effectively explore the influence of mesoscale nonuniform species distribution on target molecule diffusion behavior, and this method helps to study more realistic diffusion behavior within zeolite and improve catalyst performance.

4. METHODS

4.1. AIMD Simulation

The AIMD simulations were performed using the CP2K software package[33] at a temperature of 670 K in a constant volume and constant temperature (NVT) ensemble. The temperature was controlled by a Nosé−Hoover thermostat with three chains.[34,35] The revPBE functional was selected for the DFT calculations because of its improved performance for solid-state calculations; this functional has been extensively utilized in recent theoretical investigations of zeolite-catalyzed processes.[36,37] The combined Gaussian and Plane Wave (GPW) basis sets approach was used.[38] The DZVP-GTH basis set and pseudopotentials were used with an energy cutoff of 320 Ry,[39,40] and Grimme D3 dispersion corrections were incorporated.[41−43] A time-step of 0.5 fs was employed in the MD simulations.[44]

4.2. Blue-Moon Sampling Simulations

The free energy samplings of olefin diffusion between adjacent cages and within the cage in SAPO-34 were carried out using the blue-moon sampling method.[45−47] For the elementary diffusion processes between adjacent cages, CV is illustrated in Figure 2b, representing the height of the olefin centroid from the plane in which the 8MR window is situated. For intracage elementary diffusion processes when olefins coexist with benzene, the reaction coordinate is the olefin centroid along the z-axis, as depicted in Figure 2c. In most intracage elementary diffusion processes, the reaction coordinate (Figure 2d) is the distance difference between $d_{w_1\text{-olefin}}$ (the distance between the olefin centroid and the 8MR window centroid) and $d_{w_2\text{-olefin}}$ (the distance between the olefin centroid and the adjacent 8MR window centroid).

The constraint force F_c required to constrain the reaction coordinates at each l-value was evaluated as a function of l from individual AIMD trajectories. To obtain the diffusion free energy profiles, the potential of mean force (PMF) was calculated by integrating $\langle F_c \rangle$ over the reaction coordinate according to the following equation

$$\Delta A = \int \langle F_c \rangle \mathrm{d}l \tag{1}$$

In order to obtain accurate diffusion free energy profiles, a sampling density of 0.5 Å on the reaction coordinate was employed and each simulation was conducted for 10 ps. The initial 2.5 ps was used to equilibrate the system, and the constraint forces were collected from the last 7.5 ps. The corresponding error analysis is presented in Section S2 of Supporting Information.

4.3. Kinetic Monte Carlo Method

As mentioned above, the SAPO-34 zeolite features CHA topology, in which spacious cages are connected by small 8MR windows, with each cage containing six 8MR windows. These structural characteristics allow for the simulation of SAPO-34 zeolite using a "cubic" model, as depicted in Figure 3a.[48,49] In this model, the faces of the cube represent the 8MR windows, and olefins can diffuse through the face from one cube to an adjacent cube. Diffusion within a cube can also occur as olefins migrate from one stable adsorption site to an adjacent stable site. However, when olefins coexist with different aromatic compounds, the stable adsorption sites of olefins may change, and these details are discussed in the above sections. The distance between the centroids of the two adjacent cages is approximately 9.3 Å. Therefore, even when a 99 × 99 × 99 "cubic" model, the grid size remains representative of small SAPO-34 crystals. Most of the conclusions obtained from the current work are found to be independent of the model size, as elaborated upon in above discussions.

Experimental observations have indicated that aromatic compounds have a tendency to preferentially form at the rim of SAPO-34 zeolite catalysts.[13,14] Therefore, for the mesoscale spatial pattern of aromatic compounds within the "cubic" model, a schematic representation is presented in Figure 3b, which depicts the aromatics zones being filled from the outer subsurface layer to the innermost layer, with the same aromatic compounds occupying each cube. This distribution is referred to as the "fully filled from the outside to the inside" model. The unfilled area inside is designated as the "empty zone," while the filled area on the outside is termed the "aromatics zone." The percentage of aromatic layers is utilized as a parameter to represent the degree of filling within the model. As for the olefin species, in the initialized model, an olefin molecule is placed at the center of the "cubic" model.

After completion of the initial setup of the model, the possible diffusion processes are considered. Given that aromatic compounds are too large to diffuse into adjacent cages, they will always remain in their initial cages. Consequently, only the diffusion processes of olefins are taken into account in the subsequent analysis. The diffusion behavior of olefins between adjacent stable sites is regarded as a series of site-to-site hops, and the rate constant for each hop can be calculated from the corresponding diffusion free energy barrier obtained from the free energy profile.

There are five elementary diffusion processes to be examined: (i) diffusion from one empty cage into an adjacent empty cage (empty−empty); (ii) diffusion from one empty cage into an adjacent cage containing an aromatic molecule (empty−aromatics); (iii) diffusion from a cage containing an aromatic molecule to an adjacent empty cage (aromatics−empty); (iv) diffusion from a cage containing an aromatic molecule to an adjacent cage also containing an aromatic molecule (aromatics−aromatics); and (v) intracage diffusion when coexisting with aromatic compounds in a cage (intracage−aromatics).

The kMC iterations were performed according to the following steps:[50−57] (1) the net rate constant for all possible diffusion processes is calculated using the formula

https://doi.org/10.1021/jacsau.5c00045
JACS Au 2025, 5, 1791−1802

$$k = n_1 \times k_{\text{empty-empty}} + n_2 \times k_{\text{empty-aromatics}} + n_3 \times k_{\text{aromatics-empty}} + n_4 \times k_{\text{aromatics-aromatics}} + n_5 \times k_{\text{intra-cage}}$$

where n_1 to n_5 represent the number of diffusion directions for the specified elementary diffusion processes, and these five k_{x-x} values correspond to the diffusion rate constants of the respective elementary diffusion processes.

(2) The type of diffusion attempt that will occur is selected based on the relative weights of each process, and then the diffusion direction is selected randomly. For instance, the probability for an empty−empty diffusion process is $n_1 \times k_{\text{empty-empty}}/k$, and the diffusion direction will be selected randomly based on the probability of $1/n_1$.

(3) The selected diffusion process is then executed, modifying the position of the olefin molecule within the "cubic" model. The time interval for this attempt is calculated as $\Delta t = -\ln(x)/k$, where x is a random number between 0 and 1.

After one attempt is completed, the simulation checks whether the olefin has left the "cubic" model. If the olefin has left, the total time $t_{\text{total}} = \sum \Delta t$ is calculated and stored, and the "cubic" model is reinitialized. Otherwise, the algorithm returns to step (1) and continues the kMC simulation. The kMC simulation is terminated after 20,000 parallel tests, and the average diffusion time is then calculated. The details of the convergence test are provided in Section S5 in the Supporting Information.

4.4. Degree of Diffusion Rate Control (DDRC) Analysis

The DRC is a frequently employed concept to quantify the influence of the free energy barrier of a reaction within a complex reaction network on the overall reaction rate.[58−61] In the context of this study, this concept is adapted to gauge the effect of the free energy barrier of the elementary diffusion processes on the diffusion rate, which is referred to as the degree of diffusion rate control (DDRC), for elementary diffusion process i, its DDRC value is expressed in the following equation

$$\text{DDRC}_i = \left(\frac{\partial \ln(1/t)}{\partial(-G_{a,i}/RT)} \right)_{G_{a,j\neq i}} \quad (2)$$

where t represents the diffusion time, $G_{a,i}$ represents the diffusion free energy barrier of process i, R represents the ideal gas constant (8.314 J/(mol·K)), and T represents the temperature (670 K). The DDRC value is analogous to the DRC value, which generally ranges between −1.0 and 1.0. When the DDRC value is positive, it indicates that the higher the free energy barrier of the elementary diffusion process, the longer the diffusion time and the larger the value, the greater the influence on the diffusion time. When the DDRC value is close to 0, it suggests that the disturbance of the free energy barrier has no significant effect on the diffusion time. Conversely, when the DDRC value is negative, it implies that the higher the free energy barrier is, the shorter the diffusion time.

■ ASSOCIATED CONTENT

Supporting Information

The Supporting Information is available free of charge at https://pubs.acs.org/doi/10.1021/jacsau.5c00045.

NPT optimization of lattice parameters and the model of SAPO-34, error analysis, schematic diagram of "intra-cage-aromatics" diffusion processes, DDRC analysis, and kMC simulation convergence criteria (PDF)

■ AUTHOR INFORMATION

Corresponding Author

Bo Yang − *School of Physical Science and Technology, ShanghaiTech University, Shanghai 201210, China;* orcid.org/0000-0001-6904-6646; Email: yangbo1@shanghaitech.edu.cn

Authors

Qingteng Chen − *School of Physical Science and Technology, ShanghaiTech University, Shanghai 201210, China*

Jian Liu − *School of Physical Science and Technology, ShanghaiTech University, Shanghai 201210, China;* orcid.org/0000-0001-9576-3948

Complete contact information is available at: https://pubs.acs.org/10.1021/jacsau.5c00045

Author Contributions

Q.C. performed the AIMD simulations. J.L. performed further analyses based on AIMD simulations. B.Y. conceived the problem. All the authors contributed to writing the paper.

Notes

The authors declare no competing financial interest.

■ ACKNOWLEDGMENTS

This work was supported by the National Natural Science Foundation of China (22322302) and the National Key Research and Development Program of China (2022YFA1503804). We thank the HPC Platform of ShanghaiTech University and Shanghai Supercomputer Center for computing time.

■ REFERENCES

(1) Jiao, F.; Li, J. J.; Pan, X. L.; Xiao, J. P.; Li, H. B.; Ma, H.; Wei, M. M.; Pan, Y.; Zhou, Z. Y.; Li, M. R.; Miao, S.; Li, J.; Zhu, Y. F.; Xiao, D.; He, T.; Yang, J. H.; Qi, F.; Fu, Q.; Bao, X. H. Selective conversion of syngas to light olefins. *Science* **2016**, *351* (6277), 1065−1068.

(2) Gholami, Z.; Gholami, F.; Tišler, Z.; Tomas, M.; Vakili, M. A Review on Production of Light Olefins via Fluid Catalytic Cracking. *Energies* **2021**, *14* (4), 1089.

(3) Torres Galvis, H. M.; de Jong, K. P. Catalysts for Production of Lower Olefins from Synthesis Gas: A Review. *ACS Catal.* **2013**, *3* (9), 2130−2149.

(4) Alabdullah, M.; Rodriguez-Gomez, A.; Shoinkhorova, T.; Dikhtiarenko, A.; Chowdhury, A. D.; Hita, I.; Kulkarni, S. R.; Vittenet, J.; Sarathy, S. M.; Castaño, P.; Bendjeriou-Sedjerari, A.; Abou-Hamad, E.; Zhang, W.; Ali, O. S.; Morales-Osorio, I.; Xu, W.; Gascon, J. One-step conversion of crude oil to light olefins using a multi-zone reactor. *Nat. Catal.* **2021**, *4* (3), 233−241.

(5) Wang, C.-M.; Wang, Y.-D.; Liu, H.-X.; Xie, Z.-K.; Liu, Z.-P. Catalytic activity and selectivity of methylbenzenes in HSAPO-34 catalyst for the methanol-to-olefins conversion from first principles. *J. Catal.* **2010**, *271* (2), 386−391.

(6) Wang, C.-M.; Wang, Y.-D.; Xie, Z.-K. Insights into the reaction mechanism of methanol-to-olefins conversion in HSAPO-34 from first principles: Are olefins themselves the dominating hydrocarbon pool species? *J. Catal.* **2013**, *301*, 8−19.

(7) Hereijgers, B. P. C.; Bleken, F.; Nilsen, M. H.; Svelle, S.; Lillerud, K.-P.; Bjørgen, M.; Weckhuysen, B. M.; Olsbye, U. Product shape selectivity dominates the Methanol-to-Olefins (MTO) reaction over H-SAPO-34 catalysts. *J. Catal.* **2009**, *264* (1), 77−87.

(8) Bjørgen, M.; Svelle, S.; Joensen, F.; Nerlov, J.; Kolboe, S.; Bonino, F.; Palumbo, L.; Bordiga, S.; Olsbye, U. Conversion of methanol to hydrocarbons over zeolite H-ZSM-5: On the origin of the olefinic species. *J. Catal.* **2007**, *249* (2), 195−207.

(9) De Wispelaere, K.; Hemelsoet, K.; Waroquier, M.; Van Speybroeck, V. Complete low-barrier side-chain route for olefin formation during methanol conversion in H-SAPO-34. *J. Catal.* **2013**, *305*, 76−80.
(10) McCann, D. M.; Lesthaeghe, D.; Kletnieks, P. W.; Guenther, D. R.; Hayman, M. J.; Van Speybroeck, V.; Waroquier, M.; Haw, J. F. A complete catalytic cycle for supramolecular methanol-to-olefins conversion by linking theory with experiment. *Angew. Chem., Int. Ed.* **2008**, *47* (28), 5179−5182.
(11) Arora, S. S.; Nieskens, D. L. S.; Malek, A.; Bhan, A. Lifetime improvement in methanol-to-olefins catalysis over chabazite materials by high-pressure H2 co-feeds. *Nat. Catal.* **2018**, *1* (9), 666−672.
(12) Nawaz, S.; Kolboe, S.; Kvisle, S.; Lillerud, K. P.; Stocker, M.; Øren, H. M. Selectivity and Deactivation Profiles of Zeolite Type Materials in the MTO Process. In *Studies in Surface Science and Catalysis*; Holmen, A.; Jens, K. J.; Kolboe, S., Eds.; Elsevier, 1991; Vol. *61*, pp 421−427.
(13) Zhou, J.; Gao, M.; Zhang, J.; Liu, W.; Zhang, T.; Li, H.; Xu, Z.; Ye, M.; Liu, Z. Directed transforming of coke to active intermediates in methanol-to-olefins catalyst to boost light olefins selectivity. *Nat. Commun.* **2021**, *12* (1), No. 17.
(14) Gao, M.; Li, H.; Liu, W.; Xu, Z.; Peng, S.; Yang, M.; Ye, M.; Liu, Z. Imaging spatiotemporal evolution of molecules and active sites in zeolite catalyst during methanol-to-olefins reaction. *Nat. Commun.* **2020**, *11* (1), No. 3641.
(15) De Wispelaere, K.; Wondergem, C. S.; Ensing, B.; Hemelsoet, K.; Meijer, E. J.; Weckhuysen, B. M.; Van Speybroeck, V.; Ruiz-Martínez, J. Insight into the Effect of Water on the Methanol-to-Olefins Conversion in H-SAPO-34 from Molecular Simulations and in Situ Microspectroscopy. *ACS Catal.* **2016**, *6* (3), 1991−2002.
(16) Rojo-Gama, D.; Nielsen, M.; Wragg, D. S.; Dyballa, M.; Holzinger, J.; Falsig, H.; Lundegaard, L. F.; Beato, P.; Brogaard, R. Y.; Lillerud, K. P.; Olsbye, U.; Svelle, S. A Straightforward Descriptor for the Deactivation of Zeolite Catalyst H-ZSM-5. *ACS Catal.* **2017**, *7* (12), 8235−8246.
(17) Vogt, E. T. C.; Fu, D.; Weckhuysen, B. M. Carbon Deposit Analysis in Catalyst Deactivation, Regeneration, and Rejuvenation. *Angew. Chem., Int. Ed.* **2023**, *62* (29), No. e202300319.
(18) Pare, C. W. P.; Rzepka, P.; Hemberger, P.; Bodi, A.; Hauert, R.; van Bokhoven, J. A.; Paunović, V. Formaldehyde-Induced Deactivation of ZSM5 Catalysts during the Methanol-to-Hydrocarbons Conversion. *ACS Catal.* **2024**, *14* (1), 463−474.
(19) Yuan, J.; Gao, M.; Liu, Z.; Tang, X.; Tian, Y.; Ma, G.; Ye, M.; Zheng, A. Hyperloop-like diffusion of long-chain molecules under confinement. *Nat. Commun.* **2023**, *14* (1), No. 1735.
(20) Yang, G.; Wang, C.-M.; Li, Y.; Du, Y.-J.; Wang, Y.-D.; Xie, Z.-K. Simple structure descriptors quantifying the diffusion of ethene in small-pore zeolites: insights from molecular dynamic simulations. *Inorg. Chem. Front.* **2022**, *9* (8), 1590−1602.
(21) Cnudde, P.; Redekop, E. A.; Dai, W.; Porcaro, N. G.; Waroquier, M.; Bordiga, S.; Hunger, M.; Li, L.; Olsbye, U.; Van Speybroeck, V. Experimental and Theoretical Evidence for the Promotional Effect of Acid Sites on the Diffusion of Alkenes through Small-Pore Zeolites. *Angew. Chem., Int. Ed.* **2021**, *60* (18), 10016−10022.
(22) Smith, A. T.; Plessow, P. N.; Studt, F. Density functional theory calculations of diffusion barriers of organic molecules through the 8-ring of H-SSZ-13. *Chem. Phys.* **2021**, *541*, 111033.
(23) Cnudde, P.; Demuynck, R.; Vandenbrande, S.; Waroquier, M.; Sastre, G.; Speybroeck, V. V. Light Olefin Diffusion during the MTO Process on H-SAPO-34: A Complex Interplay of Molecular Factors. *J. Am. Chem. Soc.* **2020**, *142* (13), 6007−6017.
(24) Kaeding, W. W.; Chu, C.; Young, L. B.; Weinstein, B.; Butter, S. A. Selective alkylation of toluene with methanol to produce para-Xylene. *J. Catal.* **1981**, *67* (1), 159−174.
(25) Tian, P.; Wei, Y.; Ye, M.; Liu, Z. Methanol to Olefins (MTO): From Fundamentals to Commercialization. *ACS Catal.* **2015**, *5* (3), 1922−1938.
(26) Lezcano-Gonzalez, I.; Campbell, E.; Hoffman, A. E. J.; Bocus, M.; Sazanovich, I. V.; Towrie, M.; Agote-Aran, M.; Gibson, E. K.; Greenaway, A.; De Wispelaere, K.; Van Speybroeck, V.; Beale, A. M. Insight into the effects of confined hydrocarbon species on the lifetime of methanol conversion catalysts. *Nat. Mater.* **2020**, *19* (10), 1081−1087.
(27) Zimmermann, N. E. R.; Smit, B.; Keil, F. J. Predicting Local Transport Coefficients at Solid−Gas Interfaces. *J. Phys. Chem. C* **2012**, *116* (35), 18878−18883.
(28) Dutta, R. C.; Bhatia, S. K. Interfacial barriers to gas transport: probing solid-gas interfaces at the atomistic level. *Mol. Simul.* **2019**, *45* (14−15), 1148−1162.
(29) Le, T. T.; Qin, W.; Agarwal, A.; Nikolopoulos, N.; Fu, D.; Patton, M. D.; Weiland, C.; Bare, S. R.; Palmer, J. C.; Weckhuysen, B. M.; Rimer, J. D. Elemental zoning enhances mass transport in zeolite catalysts for methanol to hydrocarbons. *Nat. Catal.* **2023**, *6* (3), 254−265.
(30) von Ballmoos, R.; Meier, W. M. Zoned aluminium distribution in synthetic zeolite ZSM-5. *Nature* **1981**, *289* (5800), 782−783.
(31) Groen, J. C.; Bach, T.; Ziese, U.; Paulaime-van Donk, A. M.; de Jong, K. P.; Moulijn, J. A.; Pérez-Ramírez, J. Creation of Hollow Zeolite Architectures by Controlled Desilication of Al-Zoned ZSM-5 Crystals. *J. Am. Chem. Soc.* **2005**, *127* (31), 10792−10793.
(32) Ristanović, Z.; Hofmann, J. P.; Deka, U.; Schülli, T. U.; Rohnke, M.; Beale, A. M.; Weckhuysen, B. M. Intergrowth Structure and Aluminium Zoning of a Zeolite ZSM-5 Crystal as Resolved by Synchrotron-Based Micro X-Ray Diffraction Imaging. *Angew. Chem., Int. Ed.* **2013**, *52* (50), 13382−13386.
(33) VandeVondele, J.; Krack, M.; Mohamed, F.; Parrinello, M.; Chassaing, T.; Hutter, J. QUICKSTEP: Fast and accurate density functional calculations using a mixed Gaussian and plane waves approach. *Comput. Phys. Commun.* **2005**, *167* (2), 103−128.
(34) Nosé, S. A molecular dynamics method for simulations in the canonical ensemble. *Mol. Phys.* **1984**, *52* (2), 255−268.
(35) Martyna, G. J.; Klein, M. L.; Tuckerman, M. Nosé−Hoover chains: The canonical ensemble via continuous dynamics. *J. Chem. Phys.* **1992**, *97* (4), 2635−2643.
(36) Perdew, J. P.; Chevary, J. A.; Vosko, S. H.; Jackson, K. A.; Pederson, M. R.; Singh, D. J.; Fiolhais, C. Atoms, molecules, solids, and surfaces: Applications of the generalized gradient approximation for exchange and correlation. *Phys. Rev. B* **1992**, *46* (11), 6671−6687.
(37) Yang, K.; Zheng, J.; Zhao, Y.; Truhlar, D. G. Tests of the RPBE, revPBE, τ-HCTHhyb, ωB97X-D, and MOHLYP density functional approximations and 29 others against representative databases for diverse bond energies and barrier heights in catalysis. *J. Chem. Phys.* **2010**, *132* (16), 164117.
(38) Lippert, G.; Hutter, J.; Parrinello, M. The Gaussian and augmented-plane-wave density functional method for ab initio molecular dynamics simulations. *Theor. Chem. Acc.* **1999**, *103* (2), 124−140.
(39) VandeVondele, J.; Hutter, J. Gaussian basis sets for accurate calculations on molecular systems in gas and condensed phases. *J. Chem. Phys.* **2007**, *127* (11), 114105.
(40) Chen, Q.; Liu, J.; Yang, B. Identifying the key steps determining the selectivity of toluene methylation with methanol over HZSM-5. *Nat. Commun.* **2021**, *12* (1), No. 3725.
(41) Grimme, S.; Ehrlich, S.; Goerigk, L. Effect of the Damping Function in Dispersion Corrected Density Functional Theory. *J. Comput. Chem.* **2011**, *32* (7), 1456−1465.
(42) Schröder, H.; Creon, A.; Schwabe, T. Reformulation of the D-3(Becke-Johnson) dispersion correction without resorting to higher than C-6 dispersion coefficients. *J. Chem. Theory Comput.* **2015**, *11* (7), 3163−3170.
(43) Grimme, S.; Antony, J.; Ehrlich, S.; Krieg, H. A consistent and accurate ab initio parametrization of density functional dispersion correction (DFT-D) for the 94 elements H-Pu. *J. Chem. Phys.* **2010**, *132* (15), 154104.
(44) Chen, Q.; Liu, J.; Yang, B. Microenvironment of the HMOR catalyst leads to high ethylene selectivity from ketene conversion:

https://doi.org/10.1021/jacsau.5c00045
JACS Au 2025, 5, 1791−1802

Insights from ab initio molecular dynamics simulations. *Chem. Eng. J.* **2024**, *481*, 148412.
(45) Den Otter, W. K.; Briels, W. J. Free energy from molecular dynamics with multiple constraints. *Mol. Phys.* **2000**, *98* (12), 773−781.
(46) Darve, E.; Wilson, M. A.; Pohorille, A. Calculating free energies using a scaled-force molecular dynamics algorithm. *Mol. Simul.* **2002**, *28* (1−2), 113−144.
(47) Fleurat-Lessard, P.; Ziegler, T. Tracing the minimum-energy path on the free-energy surface. *J. Chem. Phys.* **2005**, *123* (8), No. 084101, DOI: 10.1063/1.1948367.
(48) Keffer, D.; McCormick, A. V.; Davis, H. T. Diffusion and Percolation on Zeolite Sorption Lattices. *J. Chem. Phys.* **1996**, *100* (3), 967−973.
(49) Hinderer, J.; Keil, F. J. Three-dimensional Monte Carlo calculations of diffusion and reaction phenomena in zeolites. *Chem. Eng. Sci.* **1996**, *51* (11), 2667−2672.
(50) Trout, B. L.; Chakraborty, A. K.; Bell, A. T. Diffusion and reaction in ZSM-5 studied by dynamic Monte Carlo. *Chem. Eng. Sci.* **1997**, *52* (14), 2265−2276.
(51) Coppens, M.-O.; Bell, A. T.; Chakraborty, A. K. Effect of topology and molecular occupancy on self-diffusion in lattice models of zeolites—Monte-Carlo simulations. *Chem. Eng. Sci.* **1998**, *53* (11), 2053−2061.
(52) Fichthorn, K. A.; Weinberg, W. H. Theoretical foundations of dynamical Monte Carlo simulations. *J. Chem. Phys.* **1991**, *95* (2), 1090−1096.
(53) Battaile, C. C. The Kinetic Monte Carlo method: Foundation, implementation, and application. *Comput. Methods Appl. Mech. Eng.* **2008**, *197* (41), 3386−3398.
(54) Lukkien, J. J.; Segers, J. P. L.; Hilbers, P. A. J.; Gelten, R. J.; Jansen, A. P. J. Efficient Monte Carlo methods for the simulation of catalytic surface reactions. *Phys. Rev. E* **1998**, *58* (2), 2598−2610.
(55) Chen, Q.; Liu, J.; Yang, B. Kinetic Monte Carlo Simulations Coupling the Isomerization and Diffusion of Xylenes in HZSM-5. *J. Phys. Chem. C* **2024**, *128* (18), 7529−7535.
(56) Zhang, W.; Guo, J.; Li, C.; Yu, Y. Theoretical insight into the polymerization of ethylene on the surface of 3A zeolite: A DFT + kMC study. *Chem. Eng. Sci.* **2023**, *281*, 119132.
(57) Xu, L.; Papanikolaou, K. G.; Lechner, B. A. J.; Je, L.; Somorjai, G. A.; Salmeron, M.; Mavrikakis, M. Formation of active sites on transition metals through reaction-driven migration of surface atoms. *Science* **2023**, *380* (6640), 70−76.
(58) Chen, S.; Zaffran, J.; Yang, B. Descriptor Design in the Computational Screening of Ni-Based Catalysts with Balanced Activity and Stability for Dry Reforming of Methane Reaction. *ACS Catal.* **2020**, *10* (5), 3074−3083.
(59) Chen, S.; Zaffran, J.; Yang, B. Dry reforming of methane over the cobalt catalyst: Theoretical insights into the reaction kinetics and mechanism for catalyst deactivation. *Appl. Catal., B* **2020**, *270*, No. 118859.
(60) Wu, P.; Yang, B. Significance of Surface Formate Coverage on the Reaction Kinetics of Methanol Synthesis from CO2 Hydrogenation over Cu. *ACS Catal.* **2017**, *7* (10), 7187−7195.
(61) Wu, P.; Yang, B. Intermetallic PdIn catalyst for CO2 hydrogenation to methanol: mechanistic studies with a combined DFT and microkinetic modeling method. *Catal. Sci. Technol.* **2019**, *9* (21), 6102−6113.

https://doi.org/10.1021/jacsau.5c00045
JACS Au 2025, 5, 1791−1802